View metadata, citation and similar papers at core.ac.uk
brought to you by CORE
provided by University of Huddersfield Repository

Non-overlap subaperture interferometric testing for large optics

Xin Wu[1,2], Yingjie Yu[1,*], Wenhan Zeng[2] , Te Qi[1], Mingyi Chen[1], Xiangqian Jiang[2]

1 Department of Precision Mechanical Engineering, Shanghai University, Shanghai 200072, China

2 Centre for Precision Technologies, School of Computing and Engineering, University of Huddersfield, Huddersfield, HD1 3DH, UK

*Corresponding author: yingjieyu@staff.shu.edu.cn

Abstract: It has been shown that the number of subapertures and the amount of overlap has a significant influence on the stitching accuracy. In this paper, a non-overlap subaperture interferometric testing method (NOSAI) is proposed to inspect large optical components. This method would greatly reduce the number of subapertures and the influence of environmental interference while maintaining the accuracy of reconstruction. A general subaperture distribution pattern of NOSAI is also proposed for the large rectangle surface. The square Zernike polynomial is employed to fit such wavefront. The effect of the minimum fitting terms on the accuracy of NOSAI and the sensitivities of NOSAI to subaperture's alignment error, power systematic error, and random noise are discussed. Experimental results validate the feasibility and accuracy of the proposed NOSAI in comparison with wavefront obtained by a large aperture interferometer and stitching surface by multi-aperture overlap-scanning technique (MAOST).

Keywords: surface reconstruction; non-overlap subaperture stitching; subaperture distribution pattern; polynomial fitting; square Zernike polynomial;

1. Introduction

The accuracy, reproducibility and efficiency of the measurement techniques and systems need to be improved with increasing demands from the optical manufacturing. Subaperture stitching interferometry plays an important role in large aperture and large NA surface metrology, including planar, spherical, aspherical and even free-form surfaces, because it can extend the lateral measurement ranges while enhancing the lateral and vertical resolutions.

In the early models of stitching interferometry, there was no overlap between subapertures[1]. In order to improve the stitching accuracy and achieve high spatial resolutions, multi-aperture overlap-scanning technique (MAOST) was proposed for high precision large aperture measurement[2,3]. With MAOST, a large optical surface is tested by an overlap-scanning sequence with a small aperture interferometer and then the surface of the full aperture is reconstructed through the consistency of data in overlapping regions. One reconstruction approach was to simultaneously make the sum of the squared differences for all overlapping data minimum to reduce the accumulation error of stitching [4]. In order to improve the accuracy, compensation using a reference mirror [5] or an iterative algorithm [6] have been proposed. These approaches have been used for large area measurement of planar[7], cylindrical[8], spherical[9] and aspherical[10] surfaces. The optimal overlap area for these methods has been shown to be 30% of the subaperture area[11]. Thus the number of subapertures will increase with the size of optics. For example, for a 400×800 mm optical flat, 66 subapertures at 30% overlapping ratio are needed if a 100 mm interferometer is used. Furthermore to ensure accuracy, the environment and the entire measurement system must be stable during scanning of these 66 subapertures making it difficult to be used in a workshop environment [12]. Hence the need arises for fewer subapertures for reduced environment uncertainty and reduced errors in the stitching process.

Two methods namely the Kwon-Thunen and Simultaneous fit [13,14] reconstruct the full aperture using

Zernike polynomial with non-overlapping subapertures but with some differences. In the Kwon-Thunen method, the subaperture wavefront and full aperture wavefront are both fitted by a Zernike polynomial and the polynomial coefficients are solved by minimizing their difference. This method is more sensitive to the alignment errors of the subapertures. In the Simultaneous fit approach, the first three Zernike terms, namely piston, x-tilt and y-tilt, of each subaperture are fitted independently, which can avoid their impact on the fitting of higher-order terms and with better computational efficiency. Though both methods suffer from the problem of describing some wavefronts with localized irregularities with the Zernike polynomials, they have sufficient precision for testing relative smooth surfaces, such as planar surfaces. The greatest advantage of this kind of method is the reduction in the number of subapertures. Using the same optical flat with the size of 400×800 mm as an example, the Kwon-Thunen or Simultaneous fit method, needs to scan about 32 subapertures saving more than 50% scanning time. Furthermore, for fewer scanning subapertures, the start-up and stop times are also reduced greatly, thus reducing mechanical errors.

This paper will test the rectangular optical flats with large scales on the machine tool table in workshop by non-overlap subaperture interferometric testing method (NOSAI). It introduces the principle of NOSAI and gives the revised Zernike polynomial suitable for rectangular shape. The effect of the minimum number of fitting terms on the accuracy of NOSAI and the sensitivities of NOSAI to subaperture alignment error, power systematic error, high frequency noise, higher-order terms of fitted surface and subapertures distribution are discussed. The experimental system is established with a dynamic interferometer as the measuring instrument. Experiments verified the feasibility and accuracy of NOSAI. In Section 2, the basic principle of NOSAI and square Zernike polynomials is described. In Section 3, a numerical simulation is given to test the validity and the sensitivities of the method. In Section 4, experimental verification of NOSAI is shown.

2. Principle of NOSAI

Assuming that the translation between subapertures is rigid and excluding geometrical errors from the mechanical platform, the measured wavefront of subapertures should be consistent with the full aperture wavefront in theory if the intererometrer is correctly calibrated. According to this principle, the fitting coefficients of piston, tip and tilt terms of subapertures and the fitting coefficients of the full aperture wavefront can be solved simultaneously. NOSAI does not involve positional relationships between subapertures, which mean that an arbitrary distribution of the subapertures is acceptable, even without overlap.

The wavefront of the full aperture surface can be expressed as,

$$W(x,y) = \sum_{i=4}^{N} m_i Z_i(x,y) \tag{1}$$

where $W(x,y)$ is the fitted wavefront of the full aperture and (x,y) is its coordinate, $Z_i(x,y)$ is the ith fitting polynomial, m_i is its coefficient, N is the total number of polynomial terms. The coefficients of the first three terms (piston, tip and tilt) are not related to the surface shape and set to zero in Eq. (1).

If there is only rigid translation between measured subaperture and full aperture wavefronts, then the residue error R can be calculated as

$$R = \sum_{k=1}^{M} [(w_k(x,y) + n_{k1} + n_{k2}x + n_{k3}y - \sum_{i=4}^{N} m_i Z_i(x,y))Q_k(x,y)]^2 \tag{2}$$

where M is the total number of subapertures, $w_k(x,y)$ is the measured wavefront of the kth subaperture, $Q_k(x,y)$ is the corresponding weight value of the kth subaperture at point (x,y) to

separate the useful sampling points ($Q_k(x,y)=1$) and the useless sampling points($Q_k(x,y)=0$). The alignment coefficients of kth subaperture relative to the full aperture is $n_k=(n_{k1},n_{k2},n_{k3})^{\mathrm{T}}$ in $X_k=(1,x_k,y_k)$.

The fitting coefficients of all subapertures are denoted as $S_n=(n_1,n_2,\cdots,n_M)^{\mathrm{T}}$, and the subaperture coordinates are $X=(X_1,X_2,\cdots,X_M)$, the fitting coefficients of the full aperture are $S_m=(m_4,m_5,\cdots,m_N)^{\mathrm{T}}$, the Zernike polynomial terms $Z=(Z_4,Z_5,\cdots,Z_N)$, the subaperture wavefronts $W=(w_1,w_2,\cdots,w_M)$ with their weights $Q=(Q_1,Q_2,\cdots,Q_M)$, then Eq.(2) can be rewritten as

$$R=\sum_{k=1}^{M}Q(W-HV)^2 \tag{3}$$

where $H=[Z\ X]$, $V=[S_m\ S_n]^T$.

By minimizing R, the least squares estimate of V is,

$$\hat{V}=(H^TQH)^{-1}H^TQW \tag{4}$$

Thus, the fitting coefficients of full aperture wavefront and alignment coefficients of each subaperture can be obtained simultaneously through a global coordinate synchronization. Thus the impact of accumulation error and local measurement errors can be reduced.

3. The measurement scheme for rectangular optical flats

For the rectangular plane surface, we attempt to program a general measurement scheme with the appropriate polynomial and the optimized subaperture distribution. This is more valuable for further application.

3.1. Square Zernike polynomial

Zernike polynomials are often used to express the wavefronts since the polynomial terms with the same forms as the aberrations observed in optical testing. It should be noted that the Zernike polynomials are orthogonal only over the unit circle. It is convenient to represent a square or rectangular aperture with 2D set of Legendre polynomials for its orthogonality, but it does not include the useful rotationally-symmetric terms, in particular, "power" term, i.e. (x^2+y^2)[15]. In ISO/TR14999, orthogonal square Zernike polynomials are built, which have the same forms as the corresponding classical Zernike polynomials but with different coefficients [16]. Due to the complex interaction between the square area of definition and the rotationally symmetrical basis of these functions, there is no simple formula for the polynomial coefficients. They can only be described term by term using the following expression,

$$\sum\{P_n(r)\cos(m\theta)\}\ \text{and}\ \sum\{Q_n(r)\sin(m\theta)\} \tag{5}$$

where (r,θ) are polar coordinates, $r=\sqrt{x^2+y^2}$. The range of x and y is $[-\sqrt{2},\sqrt{2}]$, which means half diagonal of the area should be equal to one. $P_n(r)$ and $Q_n(r)$ denote polynomials in the variable "r". and the order of the function is $n+m$, where n, m are non-negative integers.

The first 11 square Zernike polynomials based on polar symmetry are given in Table 1. Theoretically, the fitting accuracy can achieve 10^{-15} by using appropriate terms.

Table 1 Square Zernike Polynomials [16]

Term	Order($n+m$)	n	m	Polynomial
Z_1	0	0	0	1
Z_2	2	1	1	$r\cos\theta$
Z_3	2	1	1	$r\sin\theta$

Z_4	2	2	0	$2r^2-2/3$
Z_5	4	2	2	$r^2\cos 2\theta$
Z_6	4	2	2	$r^2\sin 2\theta$
Z_7	4	3	1	$r(15r^2-7)\cos\theta/5$
Z_8	4	3	1	$r(15r^2-7)\sin\theta/5$
Z_9	4	4	0	$2(315r^4-240r^2+31)/105$
Z_{10}	6	3	3	$r^3\cos 3\theta+3r(13r^2-4)\cos\theta/31$
Z_{11}	6	3	3	$r^3\sin 3\theta+3r(4-13r^2)\sin\theta/31$

3.2. Compare with normal Zernike polynomial

The most common fitting principle for the rectangular surface is using polynomials which are derived from Zernike polynomials and made orthogonal over corresponding apertures. This change should be fully transparent to the fitting process. A rectangular wavefront is simulated as Eq. (6) and fitted using two different polynomials, one is the orthogonalized Zernike polynomials, the other is the square Zernike polynomials. RMS of the residual surface error is used to illustrate the fitting accuracy. It could get 10^{-4} when using the orthogonalized Zernike polynomials (Fig.1 (a)) and get 10^{-14} when using the square Zernike polynomials (Fig.1 (b)). Both of these two polynomials could get well precision in the simulation with no error introduced. The square Zernike polynomial is a bit better than the orthogonalized Zernike polynomials and more reasonable in fitting rectangle surface.

$$W=0.3x^2+0.2x^2y^2-0.3y^2(-1\le x,y\le 1) \tag{6}$$

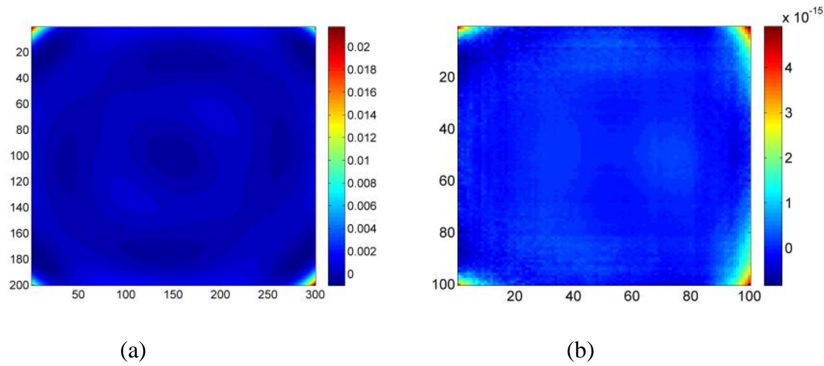

(a) (b)

Fig.1 The residual error of fitting surface using (a) the orthogonalized Zernike polynomials; (b) the square Zernike polynomials

3.3. Effect of the minimum fitting terms

The simulated full aperture surface in Cartesian coordinate with the wavelength λ is expressed as follows

$$W_0=0.3x^2+0.2x^2y^a-0.3y^2(-1\le x,y\le 1) \tag{7}$$

where a can be changed to get different surface order.

Firstly, simulate a surface with order 3 by setting a = 1, and then fit the simulated surface with different Zernike polynomials by changing the minimum fitting terms, with same sampling points in each calculation. The residual RMS of the fitted and original surface is shown in Fig.2 (a). Similarly, by simulating a surface with order 4 (a = 2), and doing the same calculation gives Fig.2 (b). From these two figures, it can be seen that the fitting error is decreased with increasing the number of Zernike terms. When the highest fitting term reaches a certain number, the residual RMS will quickly converge to the desired accuracy of 10^{-15}. Changing a to any other value gives the same conclusion. It shows that

the minimum fitting terms O and the highest order of the fitted surface in Cartesian coordinate δ satisfy the following relationship:

$$O = \delta^2 + 2 \quad (8)$$

For example, when $a = 1$, the highest order of surface δ is 3 in W_0, so the minimum fitting terms is 11 according to Eq.(8). So choosing 11 as the highest fitting term is sufficient and using higher fitting terms will not improve accuracy any more. In practice, a priori knowledge about tested surface is favorable for the polynomial order choice. And it is an effective way for inhibiting the impact of higher order terms on the reconstruction accuracy.

The sampling point does not require much. As shown in Fig.2, the trends of accuracy with 100, 600 and 1000 points are similar. Therefore, reducing the number of points in a certain range does not reduce accuracy, but improves computational efficiency.

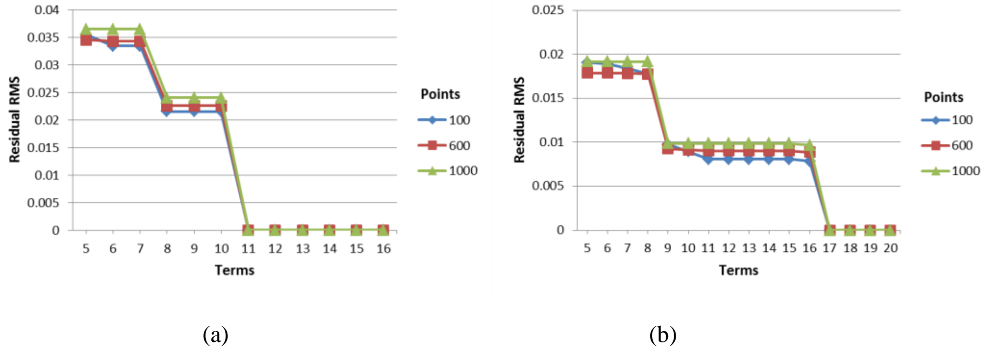

(a) (b)

Fig.2 Residual error vs. polynomial terms and sampling points: (a) 3rd order surface when a=1; (b) 4th order surface when a=2

3.4. Subapertures' amounts and distribution

A full aperture rectangular surface W_1 is simulated with square Zernike polynomials, which has 200×300 sampling points, PV 0.625 λ and RMS 0.137 λ.

$$W_1 = 0.1Z_4 - 0.2Z_5 + 0.1Z_6 \quad (9)$$

where Z_4, Z_5, Z_6 are shown in Table 1. To analyze the influence of the subaperture distribution when using NOSAI, the simulated wavefront W_1 is divided into fifteen overlapping subapertures, as shown in Fig.3, and different combinations of subapertures are selected as shown in Table 2. In these compositions, some have normal overlap between the adjacent subapertures as MAOST, some only have part overlap and some have no overlap. Random alignment errors are added in each subaperture before NOSAI calculation. Anyone subaperture could reconstruct the entire wavefront without any other errors introduced in simulation, and the accuracy of reconstruction could be 10^{-14}. But the error is unavoidable in the actual measurement, so the amount and distribution of the subapertures should be analyzed. We added a Gaussian type random noise N (0, 0.01) to each simulated subaperture, and reconstructed the wavefront with different subapertures. The PV and RMS of the residual surfaces are listed in Table 2. It can be found that the accuracy of reconstruction is decreased with reducing the number of subapertures. The subaperture distribution as Fig.4 is considered as the optimal scheme of NOSAI for the rectangle wavefront. It can be expanded as the dotted line pattern with the increase of the tested surface size. As this pattern, there is no overlap between each subapertures and the amount could be decreased a half than MAOST.

Table 2 Subaperture combination (unit: λ)

Number of subapertures	15	9	8	7	6	5	4	3
Selected subapertures	1~15	1,3,5,6,8, 10,11,13, 15	1,3,5,7,9, 11,13,15	1,3,5,8, 11,13, 15	1,3,5,11, 13,15	1,5,8, 11,15	1,5,11,15	1,5,13
Overlapping status	normal	part	non	part	non	non	non	non
Residual PV	0.0635	0.0645	0.0747	0.0782	0.0759	0.085	0.0831	0.1125
Residual RMS	0.0068	0.0068	0.0077	0.008	0.0078	0.0086	0.0085	0.0128

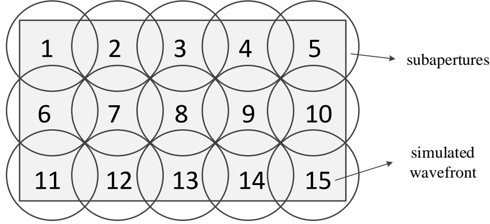

Fig.3 Subapertures distribution

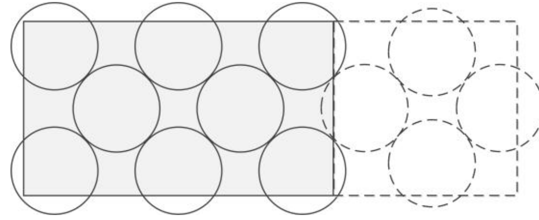
Fig.4 The general subapertures distribution pattern

4. Numerical analysis of NOSAI

Two simulated full aperture surfaces with different Zernike polynomials are chosen for analysis. The full aperture surfaces are divided into non-overlapping subapertures and then reconstructed by NOSAI. By comparing the original full aperture surface with the reconstructed results, the accuracy can be evaluated. The effect of the minimum number of fitting terms of Zernike polynomials on the reconstructed accuracy is analyzed. Then the sensitivity of residual errors on the reconstructed accuracy, including the alignment errors (piston and tilt), power error, higher-order error and high frequency noise, which may occur in the subaperture data according to the characteristics of the dynamic interferometer in the workshop environment, are discussed.

4.1. Sensitivity to subaperture alignment error

In actual testing, it is inevitable to introduce some piston and tilt alignment errors due to the straightness or verticality of the mobile platform or environmental factors. This section will analyze the suppression characteristics of NOSAI for these alignment errors.

The simulated surface W_1 in Eq. (9) is divided into six non-overlapping subapertures, as shown in Fig.5 (a). Random alignment is added to each subaperture.

$$W_{1k} = 0.1Z_{4k} - 0.2Z_{5k} + 0.1Z_{6k} + \alpha Z_{1k} + \beta Z_{2k} + \gamma Z_{3k} \tag{10}$$

where α, β, γ are random values in (-1,1). k represents the kth subaperture.

The full aperture surface is reconstructed by NOSAI. The residual surface between reconstructed result and the simulated full aperture surface is shown in Fig.5 (b), PV is 8.6×10^{-14}λ and RMS is 1.4×10^{-14} λ.

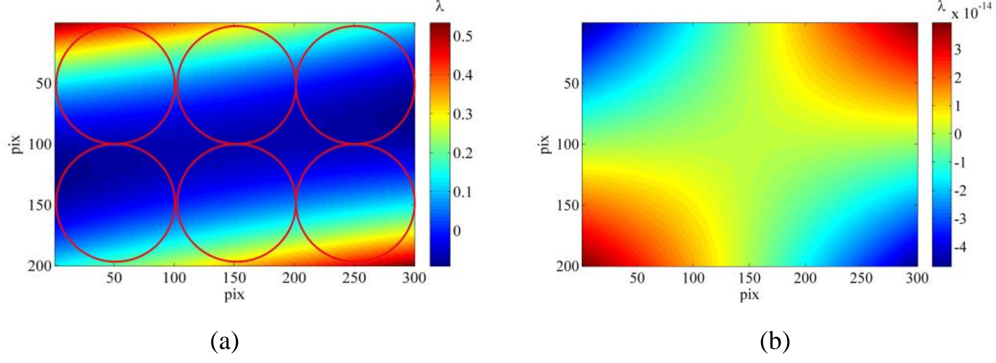

(a) (b)

Fig.5 Simulated surface W_1 and the reconstructed residual surface: (a) simulated surface W_1; (b) Residual surface

In order to verify the above conclusion, a different simulated rectangular surface W_2 is processed similarly

$$W_2 = 0.05Z_5 - 0.1Z_6 + 0.2Z_8 \tag{11}$$

Fig. 6 (a) shows the simulated surface, PV is 0.575 λ and RMS is 0.073 λ. The surface is divided into six subapertures and for each a random alignment is added as before. The residual surface is calculated and shown in Fig. 6 (b), which PV is 3.1×10^{-14} λ and RMS is 4.3×10^{-15} λ. The value of reconstructed residual error is also very small, so NOSAI can effectively calibrate the piston and tilts of subapertures and reconstruct the whole surface with high accuracy.

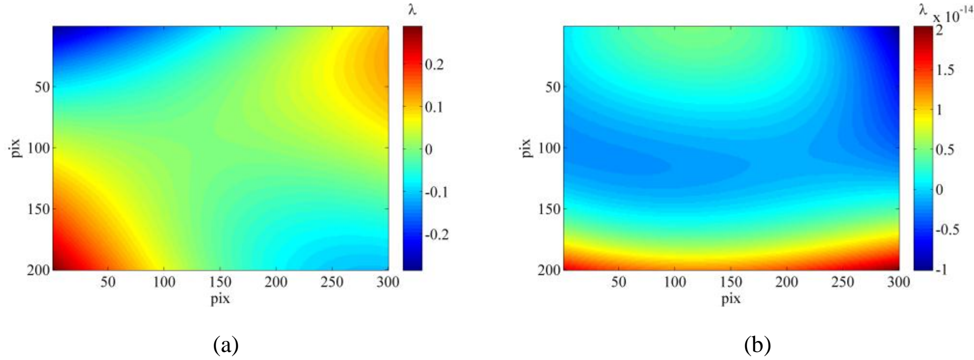

(a) (b)

Fig. 6 (a) Simulated surface W_2 and (b) the reconstructed residual surface.

4.2. Sensitivity to subaperture systematic second order error

The systematic second order error contains power and astigmatism error. In interferometry, it is one of the main systematic errors [17], especially for a dynamic interferometer with off-axis optical path design. In subaperture testing, if the systematic errors are not calibrated before testing and controlled carefully during testing, it will always affect the measurement results of each subaperture. It is obviously influence on the reconstructed result and hard to be removed completely. It is usually the same in each subaperture if the testing environment is stable.

The ideal surface, W_1, expressed in Eq. (9) above is divided into six non-overlap subapertures. A power error surface P=0.005 r^2 (PV=0.005 λ, RMS=0.002 λ) is simulated and added in each subaperture. The reconstructed result by NOSAI is shown in Fig.7 (a). The residual surface distribution is also power-type which is shown in Fig.7 (b). It means the power error will accumulate in the reconstructed process and increasing with the number of subapertures. The same situation exists in the systematic astigmatism error when the tested piece cannot rotate in testing process. It should be noted that the accumulation of systematic second order error has no relation to the profile of test surface. If the

number of the subapertures increases, the accumulated error cannot be ignored even though the value of the systematic second order error in each subaperture is small. So the subapertures' systematic second order error is the main error source in stitching measurement. The calibration before or during testing thus becomes very important and will be discussed in a future publication.

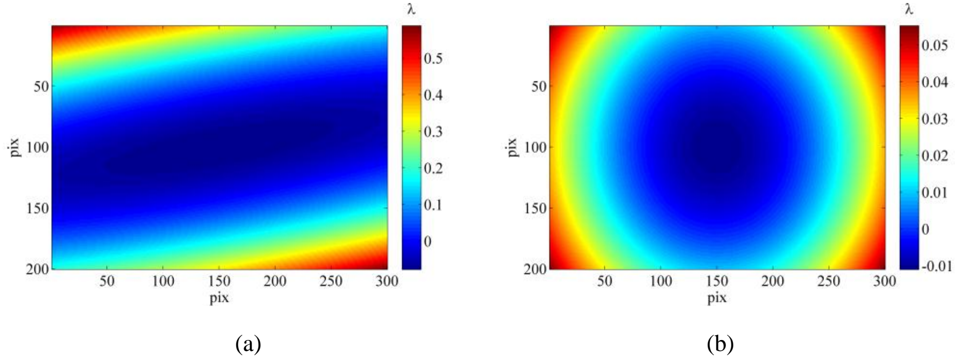

(a) (b)

Fig.7 Reconstructed results when subapertures with power error: (a) reconstructed surface (PV: 0.666λ, RMS: 0.143λ); (b) residual surface (PV: 0.066λ, RMS: 0.015λ)

4.3. Sensitivity to subaperture random noise

The accuracy of interferometry is limited by the measuring environment where random noise is inevitable. Gaussian type high frequency noise N (μ, σ^2) is added into each subaperture of W_1 (PV: 0.625 λ, RMS: 0.137 λ) to examine the sensitivity of NOSAI to the high frequency noise. Reconstructed surfaces are calculated for different values of standard deviation σ with mean value fixed at μ = 0. For each σ, 10 calculations are done and their maximum, minimum, average and standard deviation of the residual RMS are calculated and the results are shown in Fig. 8. It can be seen that the average and standard deviation of residual RMS increase with standard deviation σ, but the values of residuals RMS are less compared with the RMS of the original surface. So these graphs support the conclusion that random noise in subapertures do not accumulate significantly in the reconstructed results, and that means NOSAI has a certain degree of suppression for random noise. This is mainly because the algorithm calculates the fitting coefficients in simultaneous manner.

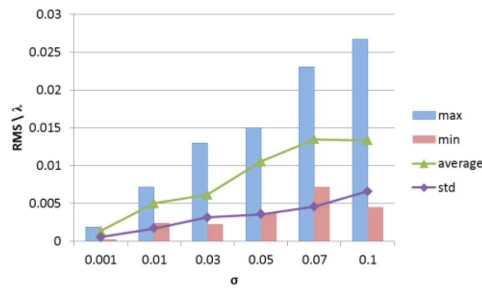

Fig. 8 Residual RMS vs. standard deviation σ (μ=0)

5. Experimental verification

In order to simulate in situ testing in workshop, an experimental system is designed on non-isolation platform in ordinary room as shown in Fig.9. A dynamic interferometer ZYGO DynaFiz™ (Middlefield, CT) with 4 inch (100 mm) aperture is used to obtain the phase data. In the testing environment, the vibration amplitude is greater than 700 nm at the frequency less than 1 Hz as tested by the interferometer's embedded measurement software. The experimental system also consists of a liftable interferometer support, a two-dimensional mobile platform, and a numerical control system.

The horizontal moving range of 2D mobile platform is 400 mm and the vertical range is 150 mm. The test sample is a K9 optical flat with 200×300×30 mm. Its full aperture wavefront is obtained by a 24-inch phase-shifting interferometer and shown in Fig.10 (a). Fig.10 (b) shows its fitting surface by the first 11 square Zernike polynomials.

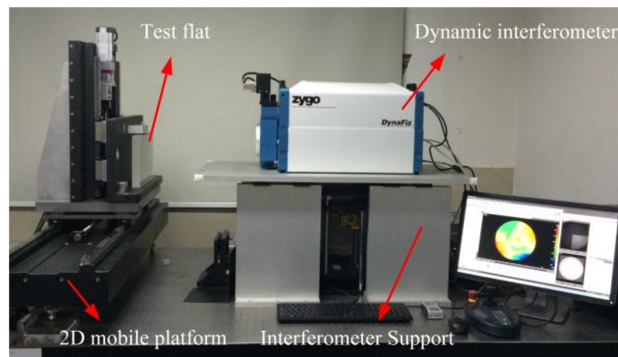

Fig.9 Experimental system

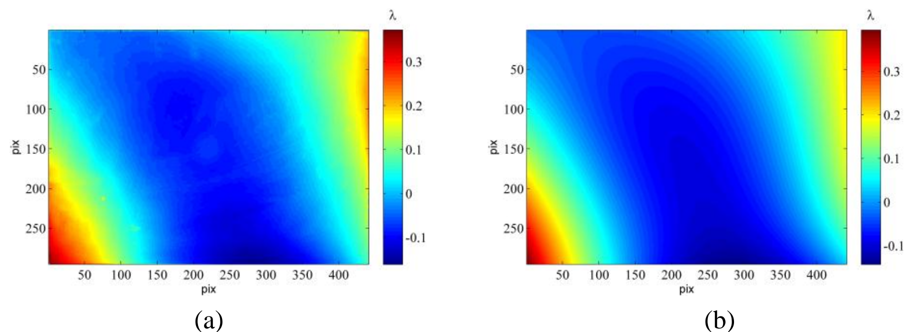

(a) (b)

Fig.10 Testing results of the sample flat with 200×300 mm: (a) Full aperture wavefront (PV: 0.534 λ, RMS: 0.092 λ); (b) fitting surface using the first 11 terms (PV: 0.538 λ, RMS: 0.091 λ)

Subapertures are arranged in 15 lattice pattern as shown in Fig.3 with a lateral overlap ratio of 30% and the vertical overlap 40%, and the resulting phase maps are seen in Fig. 11. Testing every subaperture and stitching them by MAOST, the map of stitching surface and its fitting map using the first 11 square Zernike polynomials are shown in Fig.12. Fig.13 shows the reconstructed surface obtained by NOSAI using the same subapertures. The maps of fitting surfaces obtained by MAOST and NOSAI, which are shown in Fig.12(b) and Fig.13(a), are compared and the residual map of them is showed in Fig.13 (b), which deviation is ΔPV=0.193 λ, ΔRMS=0.024 λ. That is more related to the accuracy of selected subaperture data. Generally, the difference is almost uniform and acceptable for surface shape measurement. NOSAI described here can effectively reconstruct the full aperture surface with fewer subapertures compared with the widely applied method MAOST.

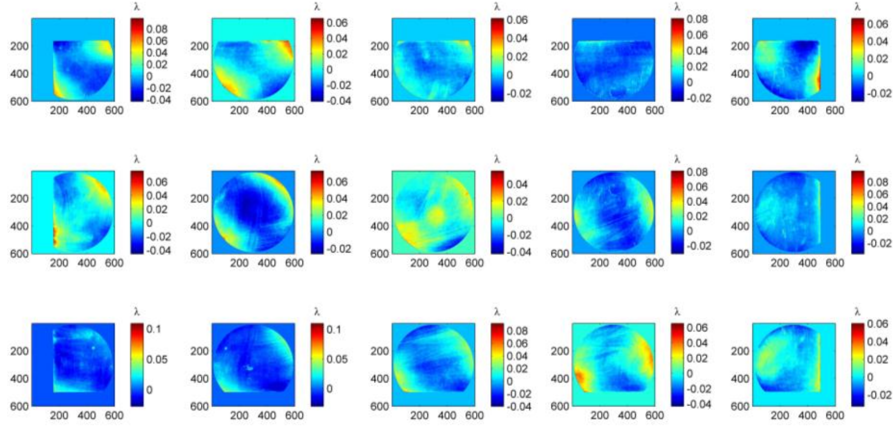

Fig. 11 Phase maps of subapertures

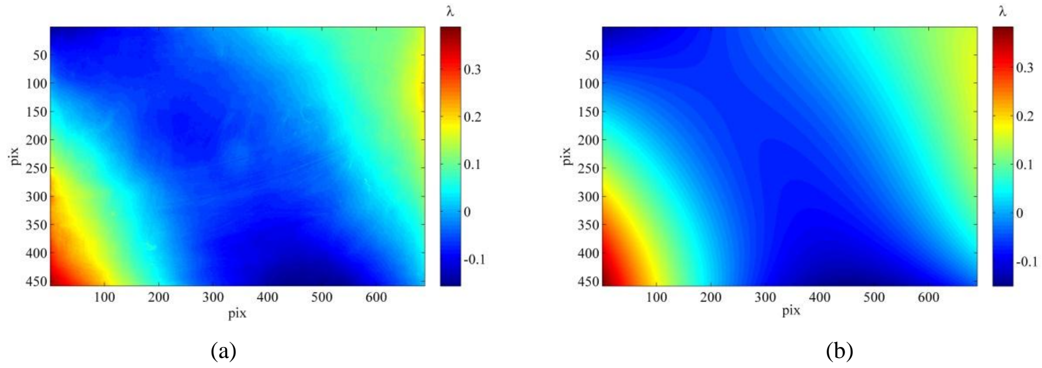

Fig.12 (a) Stitching results by MAOST (PV: 0.543λ, RMS: 0.087λ); (b) fitting surface of (a) using the first 11 square Zernike polynomials (PV: 0.535λ, RMS: 0.086λ).

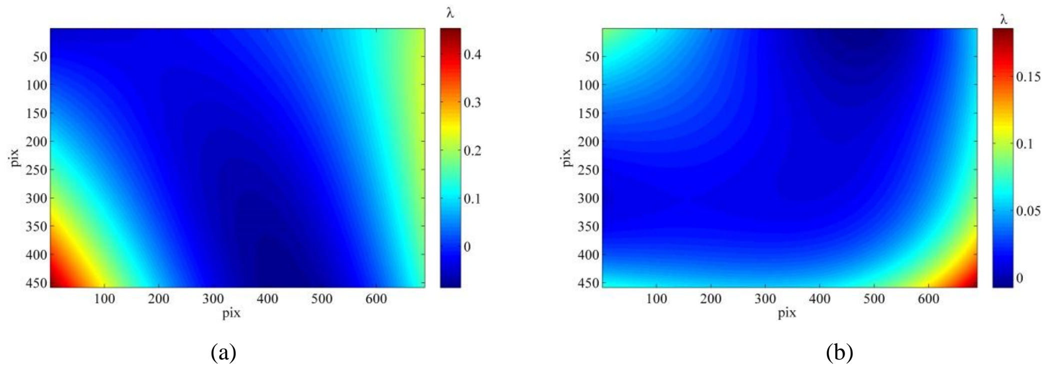

Fig.13 (a) Reconstructed surface by NOSAI (PV: 0.539λ, RMS: 0.089λ); (b) residual map of Fig.13(a) and Fig.12(b) (PV: 0.193λ, RMS: 0.024λ).

The reason why the first 11 Zernike polynomial terms were used to do fitting is explained here. The purpose of NOSAI was testing the surface shape of large optical flats. The low frequency information was enough to represent the surface shape. Furthermore, NOSAI applied in the precision grinding process, the moderate and high frequency information should be controlled in polishing process. From the algorithm perspective, the fitting results were almost consistent using more than 11 square Zernike polynomials. As illustrated in Fig. 14, 15 subapertures are calculated by NOSAI with different square Zernike terms, then compared with the fitted surface of full aperture. Consider the highest order δ of the test surface ranges from 2 to 6, then according to Eq.(7), the minimum fitting terms are equal to 6,11,18,27 and 38. It can be seen that after 11 Zernike polynomial terms, the fitting results are similar.

The maximum differences of PV and RMS in later four terms are less than 0.06 λ and 0.003 λ. Thus for surface shape testing more polynomials were not necessary by NOSAI.

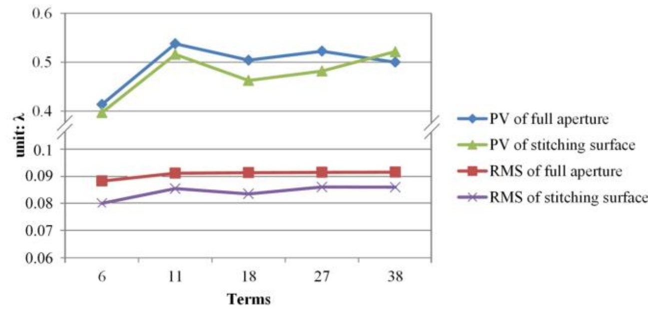

Fig. 14 Results by NOSAI with different Zernike polynomial terms

Table 3 lists the results obtained by NOSAI using different subapertures and same square Zernike terms. ΔPV and ΔRMS represent their deviations from the full aperture data. It is seen that the reconstruction with 8 subapertures gives the best result, which only need the half number of subapertures used by MAOST. As shown in Fig.15, their coefficients support the same conclusion. We compare the fitting coefficients of full aperture tested map, stitched map by MAOST and reconstructed map by NOSAI using 15 and 8 subapertures. The coefficients of 15 and 8 subapertures are approximate equal to each other, which illustrate 8 subaperture is enough for reconstructed accuracy by NOSAI. Relatively, the obvious differences are no more than 0.03 in coma and astigmatism, which corresponding the difference surface with PV 0.18 λ and RMS 0.032 λ. That means these aberrations are more sensitive to the distribution of subapertures. So a rational layout is important to enhance the stitiching accuracy while using fewer subapertures for NOSAI. Their differences with the fitting coefficients of full aperture map come from the differences of measurement instruments and environment. The proposed NOSAI used to in-situ testing the surface shape in precision grinding process, so all differences in this graph are within the acceptable range.

Table 3 Results by NOSAI using different subapertures and same square Zernike terms

Number of subapertures	15	9	8	7	6	5
Select subaperture	all	1,3,5,6,8,10 11,13,15	1,3,5,7,9,11 13,15	2,4,6,8,10 12,14	2,4,7,9,12 14	1,5,8,11,15
PV（λ）	0.521	0.462	0.532	0.543	0.577	0.450
RMS（λ）	0.086	0.077	0.093	0.085	0.099	0.079
ΔPV（λ）	0.017	0.076	0.006	0.005	0.040	0.088
ΔRMS（λ）	0.005	0.014	0.002	0.006	0.008	0.012

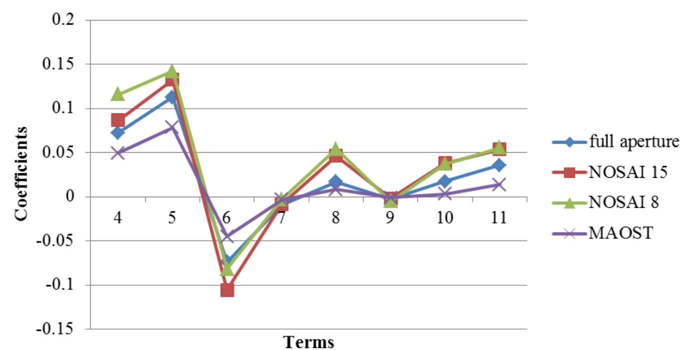

Fig.15 Comparison of the fitting coefficients obtained from full aperture, stitching map by MAOST and stitching map by NOSAI using different distributing subapertures.

6. Conclusions

The challenge in subaperture stitching for large flats in workshop is the uncertainty from long time testing in turbulent environments. Under the premise of testing accuracy, reducing the number of subapertures is an effective way to achieve in situ testing during processing. In this paper, the non-overlap subaperture interferometric testing method (NOSAI) is applied for reconstructing the wavefront of large rectangle plano optics in workshop. The square Zernike polynomial is more proper in this case. The simulation and experimental tests verify NOSAI can be used to reconstruct the low-frequency full aperture surface with fewer non-overlap subapertures. This method has its limitations, but it is very effective as a rapid in situ testing method used in the machining process. The errors we are discussing are acceptable in our application. More accurate reconstruction or error compensation methods need to be considered for higher precision measurement.

ACKNOWLEDGEMENTS

This work was performed under the support of the National Natural Science Foundation of China (NSFC) (No. 51175318) and the National Science and Technology Major Projects (No. 2013ZX04006011-217). Xin Wu (xin5star@126.com) is also thankful for the support of the China Scholarship Council to carry out research at the Centre for Precision Technologies, University of Huddersfield for one and half year.

REFERENCES

[1] C. Kim, J. Wyant. "Sub-aperture test of a large flat or a fast aspheric surface", J. Opt. Soc. Am., 71: 1587 (1981).

[2] M. Y. Chen, W. M. Cheng, and C. W. Wang, "Multiaperture overlap-scanning technique for large-aperture test". Proc. SPIE 1553, 626–635 (1991).

[3] W. M. Cheng, M.Chen. "Transformation and connection of subapertures in the multiaperture overlap-scanning technique for large optics tests." Opt. Eng. 32, 1947-1950 (1993).

[4] M. Otsubo, K. Okada, and J. Tsujiuchi. "Measurement of large plane surface shapes by connecting small- aperture interferograms". Opt. Eng. 33, 608–613 (1994).

[5] P. Su, J. H. Burge, and R. E. Parks, "Application of maximum likelihood reconstruction of subaperture data for measurement of large flat mirrors." Appl. Opt., vol. 49, no. 1, pp. 21–31, (2010).

[6] S.Y. Chen, S. Y. Li, Y. F. Dai, and Z.W. Zheng, "Iterative algorithm for subaperture stitching test with spherical interferometers." J. Opt. Soc. Am. A 23, 1219–1226, (2006).

[7] M. Bray, "Stitching interferometer for large plano optics using a standard interferometer." Proc. SPIE 3134. 39–50, (1997).

[8] J. Peng, H. Xu, Y. Yu, and M. Chen, "Stitching interferometry for cylindrical optics with large angular aperture." Meas. Sci. Technol., 26, 025204 (2015).

[9] J. Fleig, P. Dumas, P. E. Murphy, G. W. Forbes, and Q. E. D. Technologies, "An automated subaperture stitching interferometer workstation for spherical and aspherical surfaces." Proc. SPIE vol. 5188, 296–307 (2003).

[10] P. Murphy, J. Fleig, G. Forbes, D. Miladinovic, G. DeVries, and S. O'Donohue, "Subaperture stitching interferometry for testing mild aspheres." Proc. of SPIE vol. 6293, 62930J (2006).

[11] J. C. Wyant and J. Schmit, "Large field of view, high spatial resolution, surface measurements." Int. J. Mach. Tools Manuf., vol. 38, 691–698 (1998).
[12] Ziqiang Yin, Shengyi Li, Fujing Tian. "Exact reconstruction method for on-machine measurement of profile." Precision Engineering, vol. 38, 969–978, (2014).
[13] S. C. Jensen, W. W. Chow, and G. N. Lawrence, "Subaperture testing approaches: a comparison." Appl. Opt., vol. 23, 740-745, (1984).
[14] T. W. Stuhlinger, "Subaperture optical testing: experimental verification." Proc. SPIE 656, 118–127 (1986).
[15] Michael Bray. "Orthogonal polynomials: a set for square areas." Proc. SPIE 5252, 314-321(2004).
[16] ISO/TR 14999-2. Optics and photonics — Interferometric measurement of optical elements and optical systems. (2005).
[17] S. Chen, Y. Dai, S. Li, X. Peng, and J. Wang, "Error reductions for stitching test of large optical flats." Opt. Laser Technol., vol. 44, no. 5, pp. 1543–1550 (2012).